Afyon Kocatepe Üniversitesi Fen ve Mühendislik Bilimleri Dergisi

Afyon Kocatepe University Journal of Science and Engineering

AKÜ FEMÜBİD **21** (2021) 035903 (745-754) AKU J. Sci. Eng. **21** (2021) 035903 (745-754)

DOI: 10.35414/akufemubid.873404

Araştırma Makalesi / Research Article

Polaritonic Behaviors of SiC, cBN and GaN for Spectrally-Selective Nano-Optics Applications

Elif Begüm ELÇİOĞLU

Eskişehir Technical University, Faculty of Engineering, Department of Mechanical Engineering, 26555, Eskişehir, Turkey

e-mail: ebelcioglu@eskisehir.edu.tr. ORCID ID: 0000-0002-1005-4294

Geliş Tarihi: 02.02.2021 Kabul Tarihi: 07.06.2021

Keywords
Surface phonon polaritons; Figure of merit; Silicon carbide, Gallium nitride; Cubic boron nitride.

Abstract

Advances in nanotechnology enables building systems and devices with outstanding properties and functions, which makes the material aspect critically important. Materials supporting surface phonon polaritons with their resonances located in the infrared range is interesting for radiation-based energy applications, with lower optical losses exhibited compared to plasmonic materials (i.e., metals). In this work, polaritonic behaviors of three prominent phononic materials, i.e., SiC, GaN, and cBN are studied. Polaritonic figure of merit relations are analytically solved and interpreted along with the polariton propagation lengths and penetration depths. Results obtained for single material-vacuum interface revealed the highest peak magnitude of overall polaritonic figure of merit for SiC, followed by cBN, and GaN; with these merits strong dependences on materials transverse optical phonon frequencies and resonance frequencies. The results highlight the selection of the proper material to work optimally in the desired spectral range.

SiC, cBN ve GaN'ün Spektral-Seçici Nano-Optik Uygulamalar İçin Polaritonik Performanslarının Belirlenmesi

Anahtar Kelimeler
Yüzey fonon polaritonları; Performans katsayısı; Silisyum karbür; Galyum nitrür; kübik bor nitrür.

Öz

Nanoteknolojideki gelişmeler neticesinde üstün özellik ve fonksiyonlara sahip sistem ve cihazların üretimi ile, söz konusu sistemlerde kullanılacak malzemelerin seçimi kritik öneme sahip hale gelmiştir. Yüzey fonon polaritonlarını destekleyen ve rezonansları kızılötesi bölgede olan malzemeler, plazmonik alternatiflerine göre (ör: metaller) daha düşük optik kayıplar sebebiyle de ışınım tabanlı enerji uygulamaları için önem taşımaktadır. Bu çalışmada, literatürde öne çıkan üç fononik malzeme olarak SiC, GaN ve cBN'ün polaritonik davranışları incelenmiştir. Polaritonik performans katsayıları analitik olarak çözülmüş ve elde edilen polariton yayılma uzunluğu ve nüfuz derinliği sonuçları ile birlikte değerlendirilmiştir. Malzeme-vakum arayüzü için elde edilen sonuçlar, genel polaritonik performans değerinin SiC için en yüksek olduğunu, SiC'ü sırasıyla cBN ve GaN'ın takip ettiğini ve bu performans göstergelerinin malzemelerin transvers optik fonon frekansı ve rezonans frekansına bağlılığını göstermiştir. Elde edilen sonuçlar, ilgilenilen spektral aralıkta optimal performansla çalışacak malzeme seçiminin önemine atıf yapmaktadır.

1. Introduction

With the improved manipulation, handling, and fabrication of materials at the micro and nanoscale, the distinctive properties and functions of micro- and nanomaterials have become increasingly important for available and potential technological applications. Energy use with lowest possible waste and highest possible efficiency has reached to the level necessitating an urgent action to be taken due to environmental consciousness and limited sources. Thus far, this has motivated researchers to take a look at the bottom as Richard P. Feynmann suggested in his paper (Feynmann 1960) to see potential ways of employing nanomaterials, to improve efficiencies and sensitivities of processes. Thermal radiation becomes dependent on the

distance between heat-exchanging objects when they are separated by a distance smaller than the dominant emitted wavelength, i.e., $d < \lambda$ (Howell *et al*. 2021). In this case, the regime of radiative transfer is named the near-field (NF), for which the local density of electromagnetic states (LDOS) and consequently the amount of the transferred heat significantly exceeds the blackbody limit (Didari and Mengüç 2017). This increase depends on the material type of the objects, the distance between them (d), their temperatures, the environment they are held in, their shapes (Didari and Mengüç 2015) and surfaces (Chen and Xuan 2015), to name a few variables. The radiative transfer in the NF may find applications in areas including energy harvesting such as NF-thermophotovoltaics (Elçioğlu 2018), tip-based applications such as nano-manufacturing (e.g., as described by (Dönmezer 2009, Dönmezer *et al*. 2010), material characterization (e.g., with tunneling microscopy), and radiation-based thermal rectification (Park and Zhang 2013). So far, the near-field radiative transfer (NFRT) has been investigated experimentally and theoretically to unfold the mechanisms involved in this increased heat transfer. The micro-nano fabrication techniques also enabled optimizing materials to end up with higher LDOS, higher NFRT, and higher performance (e.g., as shown by (Didari and Mengüç 2017, Didari *et al.* 2018a)).

The main mechanism that makes NFRT different from that at the conventional scale (far-field, FF) is the contribution of surface modes, whose impact is negligible in the FF, as these surface (evanescent) waves having a decay length of around a wavelength (Francoeur 2010) making their contribution to FF radiation (e.g., for the objects separated by a distance much larger than the dominant emitted wavelength) negligible. In the NF, these evanescent modes can dominantly be harvested upon proper system configuration and setting. Figure 1 shows the generic NF – FF distinction based on a plane surface of a smooth slab.

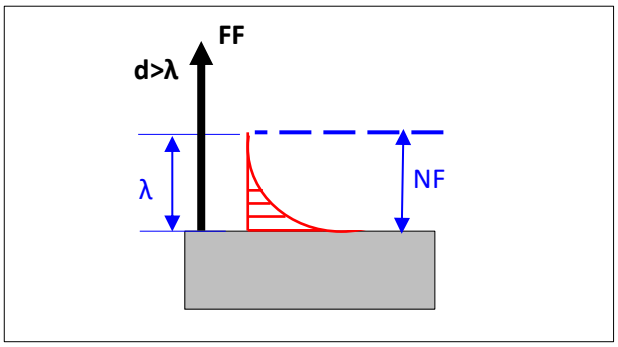

Figure 1. Near-field and far-field of a material, adapted from (Francoeur 2010).

Surface polaritons as excitations with the incident electromagnetic field, also propagate along the interface of two objects (depending on the type of materials) with decaying evanescent field in both (Francoeur 2010). The type of surface polaritons that contribute to the NFRT is surface plasmon polaritons for metals and semiconductors, and surface phonon polaritons in polar materials.

The main configurations studied in terms of the NFRT are plate-plate, sphere-plate, and sphere-sphere, all of which includes objects with a finite temperature gradient separated by a sub-wavelength distance. The most commonly investigated system setting has been parallel plates which holds potential for NF energy conversion and harvesting. The LDOS and NFRT have been investigated by covering a wide range of materials and system settings (e.g., separation, temperatures, etc.) The formulations of NFRT (as presented by (Francoeur and Mengüç 2008, Basu 2016), among others) reveal that once the separation between objects and their temperature are set, the material selection plays the major role in enhancing, or suppressing (Zhao *et al.* 2012) the NFRT. The parallel-plates configuration consists of two materials facing one another and separated by a vacuum gap. In this regard, understanding the importance of the material from its polaritonic performance at the material-vacuum interface is important.

SiC, cBN, and GaN support surface phonon polaritons in the IR, and as oppose to their plasmonic counterparts, they exhibit lower optical losses (Caldwell *et al.* 2015). This phenomenon is expected to cause a quasi-monochromatic spectral

radiative heat flux in the NF, potentially leading to higher performance (Francoeur 2010). It has been shown that the spectral NFRT flux between pairs of SiC, cBN, and GaN in parallel plates configuration exceeds the blackbody limit by orders of magnitudes (e.g., as mentioned by (Elçioğlu *et al.* 2017, Francoeur 2015) among others).

From a more materials-based point of view, performance measures for systems utilizing surface polaritons have been considered useful in conveniently assessing performance. The term figure of merit stands for a quantitative performance indicator (for a material or a system) that can be obtained more easily and conveniently than performing a whole system treatment. This applies to systems utilizing surface polaritons as well, generally by considering energy carried by polaritons, as well as their propagation and confinement. Maier (2006) mentioned a quality factor, Q, which was defined as the ratio of the energy stored to the loss per cycle; and for metals, Q was limited by the dissipative losses inside the material. It was shown that electromagnetic energy could be confined inside plasmonic cavities far below the diffraction limit, and a case study for Au half spaces was presented. More detailed figures of merit were provided for both surface plasmon polaritons and surface phonon polaritons by Caldwell et al. (2015) and comparisons were carried out to assess phononic and plasmonic materials performances by accounting for the quality factor values, locations of electrostatic resonances, and damping times. They presented figure of merit values for certain polar dielectrics, metals, metal alloys, and doped semiconductors. Berini (2006) proposed three figures of merit to quantify the spectral response of plasmon waveguides. The definition was based on a benefit-to-cost ratio where benefit was the confinement of surface plasmons, and the cost was the attenuation of them. Defining a figure of merit was considered important, since the confinement and attenuation are correlated, and there was a trade-off between them. Three figures of merit were defined for surface plasmons for a single-interface, metal slab bounded by dielectric, and dielectric slab bounded by metal cases. Configurations with Ag and SiO_2 were considered, and their figures of merit were calculated. Buckley and Berini (2007) studied three figures of merit for 2D surface plasmon waveguides and considered different shaped (narrow, wide, thin, thick) metal (Au, Ag, Al) stripes (as one, two, three, and cladded) as the configuration. Each metal considered exhibited their highest performance at a wavelength region specific to them. Ordonez-Miranda et al. (2017) developed a polaritonic figure of merit expression and provided explicit and analytical expressions for (i) single interface, and (ii) suspended thin film cases. These polaritonic figure of merits are functions of the configuration (i or ii) and the material permittivity. They also analyzed the three polaritonic figures of merit they derived considering a single interface between (i) a SiC thin film-dielectric interface, and (ii) suspended SiC thin film cases, considering two different temperatures, 295 K and 686 K, for SiC's Drude-Lorentz permittivity terms. They concluded that for SiC-dielectric interface case, the surface phonon polaritons carried more energy at around transverse optical phonon frequency (ω_{TO}) of SiC.

In order to investigate polaritonic performance from materials point of view, the fundamental material-vacuum interface case has been considered in this work. The calculation performed by Ordonez-Miranda et al. (2017) for SiC (at 295 K) has been repeated in this work for comparison purposes against the polaritonic figure of merits of cBN and GaN calculated in this current work. In this way, it is aimed to present an assessment on the polaritonic behaviors of these three very common NFRT system component, and to highlight these materials performance in spectrally selective potential nano-optics applications. For this purpose, the polaritonic figure of merit expressions as developed by (Ordonez-Miranda *et al.* 2017) have been used. By analytically solving these relations, both the energy (phonon thermal conductivity) and the phonon propagation and confinement aspects were highlighted along with the phonon propagation length and penetration depth results. To the best of the authors literature review, this paper is to first to

calculate and assess the polaritonic figures of merit of cBN and GaN, and compare to those of SiC.

2. Material and Methodology

2.1. Methodology

This work has an analytical approach in determining the polaritonic figure of merit of cBN, and GaN and comparing them with those of SiC (as previously presented by Ordonez-Miranda *et al.* (2017)) and re-calculated here for comparison purposes). Ordonez-Miranda *et al.* (2017) derived explicit analytical formulations for polaritonic figure of merit for both material-dielectric interfaces and suspended films. Here, a material-vacuum interface is considered, since vacuum environment is crucial to realize NFRT as the dominant heat exchange mechanism. The polaritonic figure of merit *Z* is the product of Z_e and Z_p, which respectively stand for the energy and propagation and confinement aspects, and defined as in Eq. (1) for material-vacuum interface (Ordonez-Miranda *et al*. 2017):

$$Z_e = \frac{\chi^2}{2\varepsilon_i},\ Z_p = \frac{\chi}{\varepsilon_i}(\varepsilon_i\eta_- - \varepsilon_r\eta_+),\quad Z = Z_e.Z_p \quad (1)$$

In Eq. (1), ε_i and ε_r are respectively the imaginary and real parts of the relative permittivity of the film material. χ and $\eta_{\pm}$ are defined as in Eq. (2) and (3) (Ordonez-Miranda *et al*. 2017):

$$\chi = \sqrt{|\varepsilon||\varepsilon+1| + |\varepsilon|^2 + \varepsilon_r} \quad (2)$$

$$\eta_{\pm} = \sqrt{|1+\varepsilon| \mp (1+\varepsilon_r)} \quad (3)$$

The penetration depth (δ) and the propagation length (Λ) of the surface phonon polaritons are calculated as in Eq. (4) and (5) (Ordonez-Miranda *et al*. 2017):

$$\delta = \frac{1}{2Re(-k_0\varepsilon/\sqrt{-1-\varepsilon})} \quad (4)$$

$$\Lambda = \frac{1}{2Im\left[k_0\sqrt{\left(\frac{\varepsilon}{1+\varepsilon}\right)}\right]} \quad (5)$$

In Eqs. (4) and (5), *Re* and *Im* denotes the real and imaginary parts of the corresponding parameter, while $k_0 = \omega/c$ where c stands for the speed of light in vacuum. It is important to note that Eqs. (1-5) are here written specifically for dielectric material-vacuum interface, and their primary versions applicable to different configurations/ cases are provided by Ordonez-Miranda *et al.* (2017).

The materials studied in this work (SiC, GaN, cBN) are known for their phononic behaviors. Polar materials support surface phonon polaritons in the IR and THz range, while exhibiting lower optical losses compared to plasmonic materials (i.e., metals) (Caldwell *et al*. 2015). Hence, realizing the behavior and performance of these common phononic materials is of importance for applications involving sub-diffraction confinement (Caldwell *et al*. 2015) and photon tunneling in the IR and THz spectral ranges.

2.2. Materials Studied in this Work

Plasmonic materials (e.g., metals) have had an important place in nano-photonics field. On the other hand, the optical losses associated with them limit their performances (Caldwell *et al*. 2015). Polar materials are known to support surface phonon polaritons (Narayanaswamy and Chen 2003) in the IR and THz range (Huber *et al.* 2008), and silicon carbide (SiC), cubic boron nitride (cBN), and gallium nitride (GaN) are among the leading phononic materials. Generation of surface phonon polaritons have found potential in microscopy and thermal emission applications, and phononic materials mostly exhibit high-temperature stability, and tunable polaritonic properties (Huber *et al*. 2008).

SiC is a wide bandgap semiconductor with high temperature stability (with a melting temperature >3000 K), high rigidity, high chemical and physical resistance (Huseynov 2020), and high breakdown field (Wondrak *et al*. 2001). GaN, similar to SiC, has high breakdown voltage and high electron velocity,

and is considered suitable in high power and high frequency applications (Mishra *et al.* 2008). GaN, as a nitride-semiconductor is also suitable for high temperature applications due to its wide energy bandgap and low carrier concentration in its undoped form (Pearton *et al*. 2002). For high-power electronics, the operating temperatures for 4H-SiC, 6H-SiC, and cBN were reported to be around 1230 K, 1200 K, and 1250 K, respectively (Lebedev and Chelnokov 1999). Apart from their individual usage, SiC and GaN can be paired for heteroepitaxial growth of GaN on SiC substrates (Talwar 2004). Cubic BN is the second hardest material and known to exhibit good thermal and chemical stability (Sharma *et al.* 2020). Bulk cBN crystals can also be doped to prepare p-type and n-type cBN (Litvinov et al. 1998), to fine-tune its properties. Due to high hardness of cBN, machining processes has been one of its prominent applications. These features combined with their phononic character makes SiC, GaN, and cBN highly worthy of investigation for nano-optics, nano-sensing, and nano-energy applications.

The frequency-dependent dielectric function of the materials is defined by the Drude-Lorentz Model, as in Eq. (6):

$$\varepsilon_r(\omega) = \varepsilon_\infty \left(\frac{\omega^2 - \omega_{LO}^2 + i\Gamma\omega}{\omega^2 - \omega_{TO}^2 + i\Gamma\omega} \right) \qquad (6)$$

In Eq. (6), ω stands for the angular frequency, while ε_∞, ω_{LO}, ω_{TO}, and Γ stand respectively for high frequency dielectric constant, longitudinal optical phonon resonance frequency, transverse optical phonon frequency, and damping factor. Values of these optical constants are provided in Table 1.

Table 1. Optical constants of the studied materials.

Material	ε_∞	ω_{LO} (rad/s)	ω_{TO} (rad/s)	Γ (rad/s)
SiC*	6.26	1.849×10^{14}	1.500×10^{14}	0.56×10^{12}
GaN**	5.3	1.41×10^{14}	1.06×10^{14}	0.0152×10^{14}
cBN***	4.46	2.4551×10^{14}	1.9887×10^{14}	9.9512×10^{11}

Constants are taken from *Ordonez-Miranda et al. (2017), for 295 K, ** Didari et al. (2018b), and *** Narayanaswamy and Chen (2003).

3. Results and Discussions

The overall polaritonic figure of merit (*Z*) calculated as in Eq. (1) for SiC, cBN, and GaN is plotted with respect to the angular frequency in Figure 2 (a). Figure 2 (b) is an alternate but more detailed version of the plot on the left (part (a)) by setting the y-axis in log-scale. It is seen that each of the materials show a single peak in their *Z* spectrum at a certain frequency. This peak is located at 1.501×10^{14} rad/s for SiC, 1.063×10^{14} rad/s for GaN, and 1.991×10^{14} rad/s for cBN. These peak locations correspond to locations very near to these materials' transverse optical phonon frequencies, i.e., ω_{TO}. As discussed by (Ordonez-Miranda *et al.* 2017) for SiC, at around ω_{TO} of the materials, surface phonon polaritons carry more energy. In addition, the dips in their *Z* spectrum (in Figure 2(b)) are located very near to the materials' ω_{LO}, such that the minima of Z appeared at 1.829×10^{14} rad/s for SiC, 1.387×10^{14} rad/s for GaN, and 2.417×10^{14} rad/s for cBN.

When the overall polaritonic figure of merit peak magnitudes are compared, it is seen that SiC has the highest, followed by cBN and then GaN. In comparison, the peak magnitude of Z value of SiC is more than 4 times greater than that of cBN, and more than 17 times greater than that of GaN.

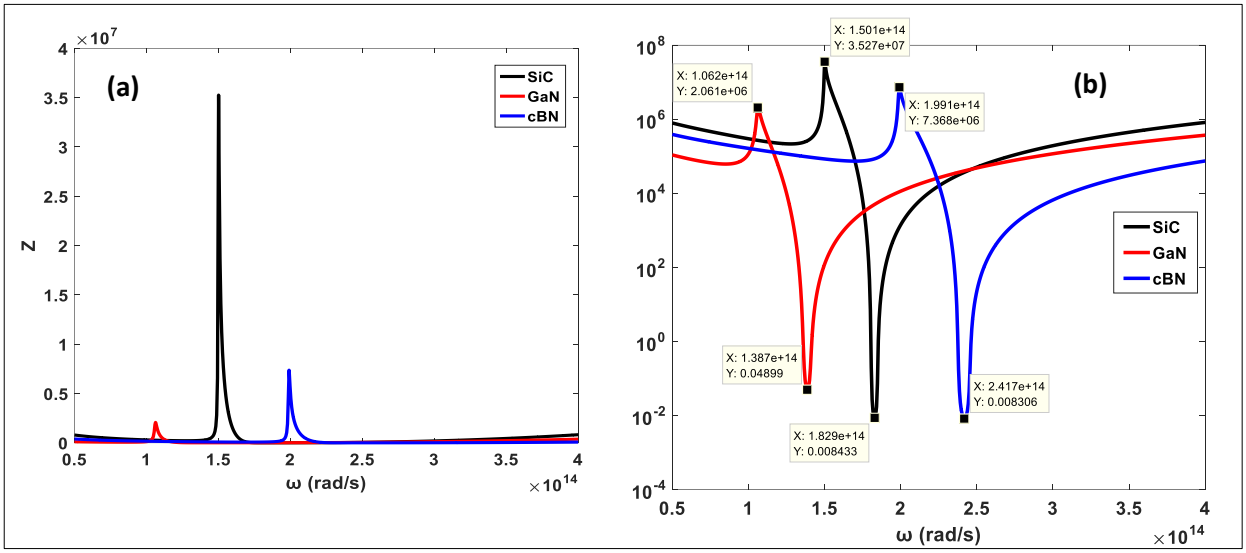

Figure 2. (a) The overall polaritonic figure of merit (*Z*) of SiC, hBN, GaN, and cBN along the material-vacuum interface, (b) the plot in part (a) with y-axis in log-scale.

One of the components of the overall polaritonic figure of merit (*Z*) is the Z_e, which relates to the capacity of the structure to enhance the polariton thermal conductivity (Ordonez-Miranda *et al.* 2017). Z_e is hence considered as the energy aspect of the overall polaritonic figure of merit. Figure 3 (a) shows the Z_e trends for SiC, GaN, and cBN. The Z_e values exhibit a minimum at 1.828x10^{14} rad/s at SiC, 1.387x10^{14} rad/s for GaN, and 2.412x10^{14} rad/s for cBN. These angular frequency values point out to another material-specific quantity, resonant frequency (ω_{res}), defined as in Eq. (7) for a single polar crystal-vacuum interface (Francoeur 2010):

$$\omega_{res} \approx \sqrt{\frac{\varepsilon_\infty \omega_{LO}^2 + \omega_{TO}^2}{\varepsilon_\infty + 1}} \tag{7}$$

With the light of the permittivity data given in Table 1 with Eq. (7), the ω_{res} values for SiC, GaN, and cBN are calculated respectively as 1.8049x10^{14} rad/s, 1.3605 x10^{14} rad/s, and 2.3765 x10^{14} rad/s.

The results presented in Figure 3 (a) can be interpreted along with the polariton propagation lengths, which relate to the ability of the polaritons to travel long distances (Ordonez-Miranda *et al.* 2017).

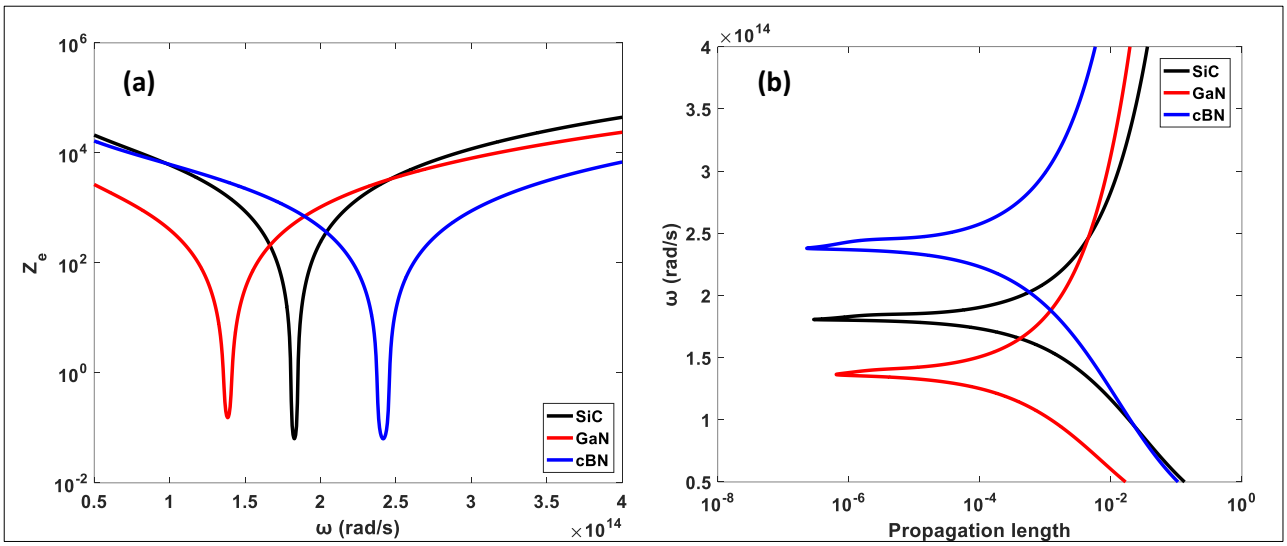

Figure 3. (a) The Z_e component of overall polaritonic figure of merit for SiC, GaN, and cBN along the material-vacuum interface, (b) the phonon propagation lengths at the SiC-, GaN-, and cBN-vacuum interface.

As shown in Figure 3 (b) the polariton propagation lengths are at their minimum around the ω_{res} calculated for SiC, GaN, and cBN for single material-vacuum interface. This points out to the fact that when polaritons propagation length is small, they are highly confined at around these frequencies. Strong confinement of surface polaritons comes with high momentum (Dubrovkin *et al.* 2020), and they reflect their evanescent decay (as in Figure 1) and highly localized nature.

The other component of the overall polaritonic figure of merit is Z_p, which relates to the ability of the structure (here, the SiC-, GaN-, and cBN-vacuum interface) to support polaritons' longitudinal propagation and transverse confinement. Figure 4 (a) depicts the Z_p trends for the studied material-vacuum interfaces. When Figure 4(b), which is the detailed version of Figure 4(a) is examined, it is seen that the peaks of Z_p are located very near the ω_{TO} of these materials, similar to the findings for overall polaritonic figure of merit, Z (in Figure 2), as also reported previously by (Ordonez-Miranda *et al.* 2017) for SiC. While this is the behavior with the Z_p maxima, the dips of Z_p are located at 1.829x10^{14} rad/s, 1.391x10^{14} rad/s and 2.415x10^{14} rad/s for SiC, GaN, and cBN, all of which are near the materials' ω_{res} values.

These results can be better interpreted considering the penetration depth results in Figure 4 (b), which shows two dips in the penetration depth results in the studied spectral range, for SiC, GaN, and cBN. Examination of Figure 4 (b) reveals that the first and second dips as marked respectively with horizontal dashed and continous lines are located at around ω_{res} and ω_{TO} values of the studied materials.

In magnitude, both the overall polaritonic figure of merit and the Z_p values are the highest for SiC-vacuum interface, followed by cBN-vacuum interface, and GaN-vacuum interface, respectively. The spectral nature of the polaritonic behavior for these settings reveal the importance of the material selection by the peaks and dips in the polaritonic figure of merits' spectral dependence on ω_{res}, ω_{TO}, and ω_{LO} values of the polar materials studied.

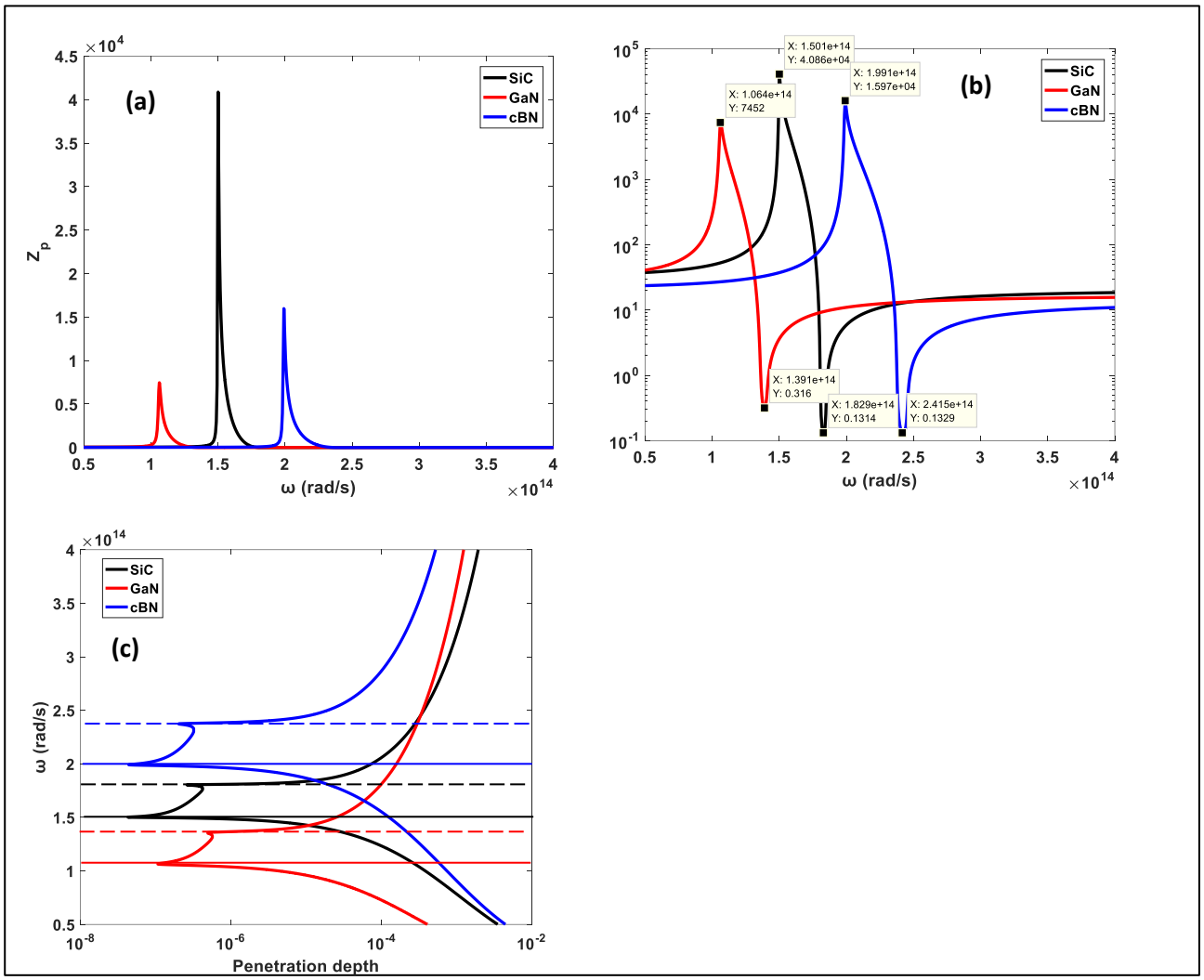

Figure 4. (a) The Z_p component of overall polaritonic figure of merit for SiC, GaN, and cBN along the material-vacuum interface, (b) the plot in part (a) with y-axis in log-scale, (c) the phonon penetration depths at the SiC-, GaN-, and cBN-vacuum interface.

4. Conclusions

In this work, the polaritonic figures of merit derived by (Ordonez-Miranda *et al*. 2017) are solved for single material (SiC, cBN, or GaN)-vacuum interface systems. Solutions for SiC at two different temperatures (i.e., 295 K and 686 K) were previously presented by (Ordonez-Miranda *et al*. 2017). In this current work, the permittivity data of SiC given for 295 K by (Ordonez-Miranda *et al*. 2017) was utilized in recalculating single interface (SiC-vacuum) results for the figures of merit. The calculations are carried out for cBN and GaN this time for Z_e, Z_p, Z, propagation length, and penetration depth. The findings for SiC are then compared to the resuts for cBN and GaN.

SiC, GaN and BN (both hexagonal and cubic BN) have been commonly investigated in NFRT systems, due to their support of surface phonon polaritons in the IR, leading to very high LDOS and spectral radiative fluxes by orders of magnitude greater than the blackbody limit at a given emitter temperature, at around the materials resonance frequency. This fact can help development of energy-efficient systems that are needed today and in the future. To the best of the authors knowledge, this work is the first to present polaritonic behavior of GaN and cBN, and compare them to those of SiC. Results showed that both Z_p and Z exhibited the highest peak magnitude for SiC, followed by cBN and then GaN, at around the resonance frequencies of these materials. The overall polaritonic figure of merit of SiC is greater

than that of cBN by more than 4 times. The peak magnitudes of the overall figure of merit (*Z*) for SiC, cBN, and GaN are calculated respectively as 3.527×10^7, 7.368×10^6, and 2.061×10^6, centered around very near these materials' ω_{TO}. The dips in the *Z* spectrum are also material-specific, as they are located very near to the materials' ω_{LO}. When it comes to Z_p component of the overall polaritonic figure of merit, *Z*, it is seen that the peak magnitude for SiC, cBN, and GaN are 4.086×10^4, 1.597×10^4, and 7.452×10^3, centered around very near these materials' ω_{TO}. The dips in the Z_p spectrum are also material-specific, as they are located very near to the materials' ω_{res}.

This single interface (dielectric material-vacuum) system setting is fundamentally important as it involves one material and vacuum, fully reflecting the impact of the materials nature on the polaritonic performance. This is because polaritonic behavior of textured/corrugated surfaces and multi-layers (Didari *et al.* 2018a) implicitly include the effects of presence of such thin layers and nano-elements on the surfaces, their thicknesses, shapes, etc., in addition to the sole effect of the material. It is therefore important to understand the sole influence of the materials themselves in this fundamental configuration to develop new and more efficient systems. The results indicate that these merits are strongly influenced by the material type (and hence the materials dielectric properties) such that the performance merits' maximum and minimum points are located very near the ω_{res}, ω_{TO} and ω_{LO} values of the materials. Considering the fact that these semiconductors can be doped/ mechanically modified to fine-tune their properties, and the technological nano-patterning opportunities, the material(s) can be selected with the desired polaritonic behavior, including optimum polariton propagation and confinement, for their potential use in opto-electronics, sensing, characterizing, and harvesting nano-devices. Such polaritonic performance evaluations of materials (both plasmonic and phononic) are expected to provide solid insight on development of systems including those harvest energy (e.g., NFRT), utilize surface polariton (plasmon, phonon, hybrid) resonance.

5. References

Basu, S. 2016. Near-Field Radiative Heat Transfer across Nanometer Vacuum Gaps: Fundamentals and Applications, Elsevier, 119-264.

Berini, P., 2006. Figures of Merit for Surface Plasmon Waveguides, *Optics Express*, **14,** 26, 13030–42.

Buckley, R., P. Berini., 2007. Figures of Merit for 2D Surface Plasmon Waveguides and Application to Metal Stripes, *Optics Express*, **15**, 19, 12174–82.

Caldwell, J. D. et al., 2015. Low-Loss, Infrared and Terahertz Nanophotonics Using Surface Phonon Polaritons, *Nanophotonics,* **4,** 44-68.

Chen, Y., and Xuan, Y., 2015. The Influence of Surface Roughness on Nanoscale Radiative Heat Flux between Two Objects, *Journal of Quantitative Spectroscopy and Radiative Transfer,* **158**, 52–60.

Didari, A., Elçioğlu, E.B., Okutucu Özyurt, T. and Mengüç, M.P., 2018a. Near-Field Radiative Transfer in Spectrally Tunable Double-Layer Phonon-Polaritonic Metamaterials, *Journal of Quantitative Spectroscopy and Radiative Transfer,* **212,** 120-127.

Didari, A., Elçioğlu, E.B., Okutucu-Özyurt, T., and Mengüç, M.P., 2018b. Tailoring Near-Field Thermal Radiation with Mesoporous GaN and h-BN Designer Metamaterials, in *Eurotherm Seminar 110 – Computational Thermal Radiation in Participating Media - VI*, Cascais, Portugal.

Didari, A., and Mengüç. M. P., 2015. Near-Field Thermal Emission between Corrugated Surfaces Separated by Nano-Gaps, *Journal of Quantitative Spectroscopy and Radiative Transfer,* **158**, 43–51.

Didari, A. and Mengüç, M.P., 2017. A Design Tool for Direct and Non-Stochastic Calculations of near-Field Radiative Transfer in Complex Structures: The NF-RT-FDTD Algorithm. *Journal of Quantitative Spectroscopy and Radiative Transfer,* **197**, 95–105.

Dönmezer, F. N. 2009. A Numerical Study on Dependent Absorption and Scattering by Interacting Nanosized Particles, M.Sc. Thesis, Middle East Technical University, The Graduate School of Natural and

Applied Sciences, 99.

Dönmezer, F. N., Mengüç, M.P., and Okutucu, T., 2010. Dependent Absorption and Scattering by Interacting Nanoparticles. in *6th International Symposium on Radiative Transfer (RAD10)*, Antalya, Turkey.

Dubrovkin, A.M. et al., 2020. Resonant Nanostructures for Highly Confined and Ultra-Sensitive Surface Phonon-Polaritons, *Nature Communications,* **11,** 1863, 1–7.

Elçioğlu, E. B. 2018. Fabrication of Silicon Carbide-on-Silicon Based Devices for Effective Near-Field Thermal Radiation Transfer, PhD Thesis, Middle East Technical University, The Graduate School of Natural and Applied Sciences, 183.

Elçioğlu, E. B., Didari, A., Okutucu-Özyurt, T., and Mengüç, M.P., 2017. GaN-SiC Katmanlı Nano-Yapılar ve Yakın-Alan Işınımına Sıcaklık Farkı ve Mesafenin Etkileri, in *21. Ulusal Isı Bilimi ve Tekniği Kongresi ULIBTK'17 Bildiriler Kitabı*, Çorum, Turkey.

Feynmann, R., 1960. There's Plenty of Room at the Bottom. *Engineering and Science,* **23**(5): 22–36.

Francoeur, M., and Mengüç, M.P., 2008. Role of Fluctuational Electrodynamics in Near-Field Radiative Heat Transfer. *Journal of Quantitative Spectroscopy and Radiative Transfer,* **109**(2), 280–93.

Francoeur, M. 2010. Near-Field Radiative Transfer: Thermal Radiation, Thermophotovoltaic Power Generation and Optical Characterization, PhD Thesis, University of Kentucky, The Graduate School, 323.

Francoeur, M., 2015. Nanostructures Feel the Heat, *Nature Nanotechnology,* **10**, 206-208.

Howell, J.R., Mengüç, M.P., Daun, K., and Siegel, R., 2021. Thermal Radiation Heat Transfer. 7th Edition, Boca Raton, FL: CRC Press, Taylor & Francis Group, 741-774.

Huber, A. J., Deutsch, B., Novotny, L. and Hillenbrand, R., 2008. Focusing of Surface Phonon Polaritons, *Applied Physics Letters* **92**, 203104.

Huseynov, E.M., 2020. Thermal Stability and Heat Flux Investigation of Neutron-Irradiated Nanocrystalline Silicon Carbide (3C – SiC) Using DSC Spectroscopy, *Ceramics International,* **46**, 5645–48.

Lebedev, A. A, and Chelnokov, V.E., 1999. Wide-gap semiconductors for high-power electronics, *Semiconductors*, **33**(9), 999-1001.

Litvinov, D., Taylor II, C. A., Clarke, R., 1998. Semiconducting cubic boron nitride, *Diamond and Related Materials*, **7**, 360—364.

Maier, S.A., 2006. Effective Mode Volume of Nanoscale Plasmon Cavities, *Optical and Quantum Electronics* **38**, 257–67.

Mishra, U.K.M., Shen, L., Kazior, T.E. and Wu, Y.-F., 2008. GaN-Based RF Power Devices and Amplifiers, *Proceedings of the IEEE,* **96**(2): 287–305.

Narayanaswamy, A. and Chen, G., 2003. Surface Modes for near Field Thermophotovoltaics, *Applied Physics Letters*, **82**(20), 3544-3546.

Ordonez-Miranda, J., et al. 2017. ,Polaritonic Figure of Merit of Plane Structures., *Optics Express* **25**(21): 25938–25950.

Park, K. and Zhang, Z., 2013. Fundamentals and Applications of Near-Field Radiative Energy Transfer, *Frontiers in Heat and Mass Transfer,* **4**, 013001.

Pearton, S.J., et al., 2002, New applications advisable for gallium nitride, *Materials Today,* **5**(6), 24-31.

Sharma, V., et al., 2020. Thermal Transport Properties of Boron Nitride Based Materials: A Review, *Renewable and Sustainable Energy Reviews*, **120**, 109622.

Talwar, D. N., 2004. Lattice Dynamics of Defects and Thermal Properties of 3C-SiC, in SiC Power Materials (Ed: Feng, Z. C.), Springer-Verlag Berlin Heidelberg, 161-208.

Wondrak, W., et al., 2001. SiC Devices for Advanced Power and High-Temperature Applications, *IEEE Transactions on Industrial Electronics*, 48(2), 307-308.

Zhao, Y., Tang, G.H., and Li, Z.Y., 2012. Parametric Investigation for Suppressing Near-Field Thermal Radiation Between Two Spherical Nanoparticles, *International Communications in Heat and Mass Transfer,* **39**, 918–922.